

ORIGINAL PAPER

T. D. Archer · S. E. A. Birse · M. T. Dove  
S. A. T. Redfern · J. D. Gale · R. T. Cygan

## An interatomic potential model for carbonates allowing for polarization effects

Received: 31 October 2001 / Accepted: 21 June 2002

**Abstract** An empirical model for investigating the behaviour of  $\text{CaCO}_3$  polymorphs incorporating a shell model for oxygen has been created. The model was constructed by fitting to: the structure of aragonite and calcite; their elastic, static and high-frequency dielectric constants; phonon frequencies at the wave vectors  $[1/2 \ 0 \ 2]$  and  $[0 \ 0 \ 0]$  of calcite; and vibrational frequencies of the carbonate deformation modes of calcite. The high-pressure phase transition between calcite I and II is observed. The potentials for the  $\text{CO}_3$  group were transferred to other carbonates, by refitting the interaction between  $\text{CO}_3$  and the cation to both the experimental structures and their bulk modulus, creating a set of potentials for calculating the properties of a wide range of carbonate materials. Defect energies of substitutional cation defects were analyzed for calcite and aragonite phases. The results were rationalized by studying the structure of calcite and aragonite in greater detail.

**Keywords** Calcite · Aragonite · Empirical interatomic shell

### Introduction

Carbonates form an important group of minerals of relevance to many aspects of Earth sciences due to their

abundance on the Earth's surface, in both biogenic and inorganic precipitates and in sedimentary rock. Examples of areas in which a deeper understanding of carbonates is needed include building a fundamental understanding of isotope fractionation ( $^{12}\text{C}/^{13}\text{C}$  and  $^{16}\text{O}/^{18}\text{O}$ ) in geochemistry, the study of the carbonate phase diagram and elucidating the transport properties of cations within carbonates, which are necessary for the evaluation of the order/disorder relations (Dove and Powell 1989, Dove et al. 1992a).

Trends are observed in the defect concentration and isotope fractionation ( $^{12}\text{C}/^{13}\text{C}$  and  $^{16}\text{O}/^{18}\text{O}$ ) of isotopes in biogenic calcite and aragonite with time, water depth and temperature. Variations in oxygen isotope fractionation may be linked to variations in ocean temperature and salinity, while changes in carbon isotope fractionation have been associated with ocean circulation variations (Bigg and Rohling 2000). These observed trends are used as a proxy to infer environmental conditions at the time when the materials were created. The particular polymorph produced also depends on environmental conditions. Although trends are observed, the fine detail of the atomic-scale processes that cause the trends are not understood. The aim in this study was to model the behaviour of defects in carbonate structure with the hope of shedding further light on these atomic-scale processes and to gain a better understanding of the high-pressure phase diagram of calcite.

There are several polymorphs of calcium carbonate but even though it is one of the most abundant minerals, aspects of the phase diagram still remain unknown. At zero pressure and zero temperature and pressure, the rhombohedral calcite I structure is stable. As pressure is applied, calcite I undergoes a first-order phase transition to the monoclinic calcite II structure at 1.45 GPa (Singh and Kennedy 1974). A further phase transition occurs to calcite III at 2.2 GPa (Merrill and Bassett 1975). Although the existence of calcite III has been reported in many papers (Merrill and Bassett 1975; Smyth and Ahrens 1997), the crystal structure and many of its properties are still unknown.

T. D. Archer · S. E. A. Birse · M. T. Dove  
S. A. T. Redfern (✉)  
Department of Earth Sciences,  
University of Cambridge,  
Downing Street, Cambridge, CB23EQ U.K.  
e-mail: satr@esc.cam.ac.uk

J. D. Gale  
Department of Chemistry,  
Imperial College of Science, Technology and Medicine,  
South Kensington, London, SW7 2AY, U.K.

R. T. Cygan  
Geochemistry Department,  
Sandia National Laboratories,  
Albuquerque, New Mexico 87185-0750, U.S.A.

Previous empirical computational studies on CaCO<sub>3</sub> (Dove et al. 1992b; Pavese et al. 1992; Catti et al. 1993, 1996; Fisler et al. 2000) included extensive testing of rigid ion and, more recently, shell models of the calcite and aragonite lattices. Basic properties such as elastic and optical properties have been calculated.

Catti et al. 1993 and Pavese et al. 1992 created rigid ion models for both calcite and aragonite and a rudimentary shell model. Although the potentials worked well for the polymorph they were designed for, they were not interchangeable or transferable. The coefficients of the interaction functions were separately fitted to the structure and properties of calcite and aragonite. Transferring the coefficients generated for one structure to the other does not produce reasonable results. This suggests that the potentials do not closely represent the real forces observed when the crystal is distorted, for example, with a defect.

Dove et al. (1992b) created a rigid ion model for CaCO<sub>3</sub>, which was fitted to the structure and properties of aragonite and calcite. The predicted properties compared well with experimental parameters including the phonon dispersion along [1 0 4] and [0 0 1] directions of the calcite lattice.

Although rigid ion models work well to reproduce the bulk properties of a material, they do not work well for defects. In real crystals, the presence of a defect causes the surrounding atom nuclei to move but the degree of movement is cushioned by polarization effects. If the atoms cannot polarize, the surrounding stress field will be unrealistically large. We attempted to transfer the rigid ion model created for CaCO<sub>3</sub> by Dove et al. (1992b) by refitting the C–O Buckingham potential to the structure and bulk modulus of magnesite, rhombohedral MgCO<sub>3</sub>. No stable structure could be found, suggesting that the rigid ion models do not offer enough flexibility to reproduce carbonates of other compositions and therefore cannot be used to model defects. The recent addition of a relaxed fitting algorithm to GULP (Gale 1997) allows shell models to be created which take into account polarization effects, and we have exploited this to generate an improved transferable set of potentials for modelling carbonates.

The model produced in the paper by Catti et al. (1996) incorporates an oxygen shell to allow polarization of the CO<sub>3</sub> group. It is able to reproduce the experimental structures of calcite I, calcite II and aragonite. The model was used to calculate the elastic constants and structural features as a function of temperature.

A more recent model for calcite has been reported by Fisler et al. (2000). This model reproduces the data from which it was created with a high degree of accuracy. However, the structure of calcite I produced by this model is unstable, due to imaginary phonon frequencies of wave vectors away from the zone centre, in particular the soft mode of the calcite I–II transition at the wave vector (½ ½ 1). An imaginary phonon frequency corresponds to a motion at a potential energy maximum

rather than a potential minimum. Calculations of the structure using models with negative phonon frequencies can appear to be stable in a given unit cell, but would lead to distortion in an appropriately large supercell.

The imaginary phonon frequency at the wave vector [½ 0 2] is the soft mode of the pressure-induced calcite I–II phase transition. It is interesting to note that application of negative pressures was unable to remove this instability. Although Fisler's model is unstable, the potential structure is a good starting point from which to create a new and improved model. As in the work by Fisler et al. (2000), the model has been fitted to the structures of aragonite and calcite, the elastic, static and high-frequency dielectric constants, the vibrational frequencies of the carbonate deformation modes of calcite. In addition, several phonon frequencies were included at both the [½ 0 2] and [0 0 0] points of the Brillouin zone of calcite. The model was used to analyze the energy of defects in the aragonite and calcite structures and to investigate the pressure-induced phase transitions of calcium carbonate.

## Development of an empirical model

The simulations performed in this study use the GULP code (Gale 1997). The GULP code implements amongst other interatomic potentials the Born model description (Born and Huang 1954) that treats the ionic material as a collection of point ions with electrostatic and short-range forces acting between them. The short-range energy contribution due to interactions between each particle and all others is summed within a predetermined cutoff. The contribution of the long-range electrostatic forces is summed using the Ewald sum (Jensen 2002).

Fitting an empirical model involves minimizing the sum of squares between experimental and calculated parameters by changing the empirical coefficients. Previous algorithms for calculating the polarization effects do not allow the structure to reach a stable state where the forces are zero, before calculating a perturbation to the coefficients. The "relaxed fitting" algorithm (Gale 1996) available within GULP finds the energy minimum of a structure by displacing the atoms and atom shells. Properties and structural displacements are calculated and compared with the experimental values, allowing the Newton–Raphson algorithm to make changes to the empirical parameters. By allowing the structure to relax, before changing the coefficients, the polarization of the oxygen is taken into account.

We used the form of the potentials from the paper of Fisler et al. (2000), which splits the oxygen into two entities: a core and a mass-less shell, each with a corresponding charge. A spring potential acts to model the interaction between the oxygen core and the shell.

$$U(r) = \frac{K_2 r^2}{2} + \frac{K_4 r^4}{24} . \quad (1)$$

During fitting, the parameter  $K_4$  was fixed at the value determined in the previous study (Fisler et al. 2000), while  $K_2$  was allowed to vary. The relaxed fitting algorithm allows the shell to move relative to its core to create a dipole. This reproduces the polarization of the oxygen atom. The Coulomb interaction is excluded within each  $\text{CO}_3$  group.

Potentials that act on the  $\text{CO}_3$  group from outside interact with the oxygen shell; these include a Buckingham O–O and a cation–O interaction. The  $A$ ,  $C$  and  $\rho$  are parameters of the Buckingham function are optimized during fitting.  $r$  is the interatomic distance.

$$U(r) = Ae^{-r/\rho} - Cr^{-6}. \quad (2)$$

Potentials associated with interactions between atoms of the same  $\text{CO}_3$  group act on the oxygen core. These are an O–O Buckingham interaction and a C–O Morse interaction. For the Morse interaction the  $A$  and  $D$  values are optimized by fitting,  $r_0$  is the predetermined bond length and  $r$  is the distance between atoms.

$$U(r) = D \left\{ \left[ 1 - e^{-A(r-r_0)^2} \right]^2 - 1 \right\}. \quad (3)$$

The model also contains a three-body term, to maintain the  $120^\circ$  bond angle in the  $\text{CO}_3$  group.  $K_2$  is optimized during fitting,  $\theta$  is the bond angle.

$$U(\theta) = \frac{K_2}{2} (\theta - 120^\circ)^2. \quad (4)$$

The potential energy associated with the out-of-plane displacement of C within the  $\text{CO}_3$  group has also been incorporated in the model. This depends on the improper torsional angle  $\phi$ , between  $\text{OCO}'$  and  $\text{OCO}''$  planes, the  $K$  parameter is determined during fitting.

$$U(\phi) = K[1 - \cos(2\phi)]. \quad (5)$$

The values of the empirical coefficients and the charges were determined using the “relaxed fitting” algorithm of GULP. The model was fitted to the structures of aragonite and calcite, the elastic, static and high-frequency dielectric constants of both polymorphs, the phonon frequencies at the  $[1/2 \ 0 \ 2]$  and  $[0 \ 0 \ 0]$  points in the Brillouin zone of calcite and vibrational frequencies of the carbonate deformation modes of calcite. During fitting, it was necessary to weight the experimental results. The experimental data were weighted during fitting to take into account experimental errors for each parameter, taking care not to produce a few highly accurate results at the expense of other parameters. For example, we found that heavily weighting the crystal structures would be at the expense of the phonon frequencies, so the weighting on the structures was reduced.

Internal energy minimizations were performed at constant pressure allowing all individual ionic coordinates and lattice parameters to vary, while constraining the space-group symmetry. The charge of the Ca ion was held fixed at  $2+$  to allow for later defect substitution. Although thermal effects are not taken into account in the model, the temperature of the system is biased

towards room temperature by fitting data from room-temperature experiments.

The model described in the paper by Fisler et al. (2000) reproduces experimental structural data with a high degree of accuracy, but does so at the expense of the stability of the structure. We have reduced the accuracy of the fit to produce a stable model, as given in Table 1. Table 2 shows how well the potentials created reproduce experimental data. The deviation of the elastic constants from the experimental results is not large enough to cause the crystal to distort unrealistically when pressure is applied. The main mechanism of structural change comes from the pressure induced soft mode which is best observed through the phonon distribution curves. The phonon dispersion curves were calculated between the gamma point and the wave vector  $[1/2 \ 0 \ 2]$ , as given in Fig. 1, and the gamma point and  $[0 \ 0 \ 1.5]$ , shown in Fig. 2. Although the dispersion curves were not used during the fitting, they still show the basic features of the experimental curves with a small systematic error.

### High-pressure phase transition

Experiment shows that the high-pressure, low-temperature, transition from rhombohedral calcite I to the monoclinic calcite II polymorph results in two displacements. First, there is an  $11^\circ$  rotation in the opposite direction to the adjacent carbonate group along the  $c$  axis and second small anti-parallel displacement of adjacent Ca ions occur (Redfern and Angel 1999). The structural nature of the further high-pressure transition to calcite III and its structure are unknown.

The behaviour under pressure of the models produced by Dove et al. (1992b) and Pavese et al. (1996) and the potential generated in this study were analyzed using a large supercell. Each model has at least three stable phases: calcite I, calcite II and a high-pressure phase. In rhombohedral calcite I the carbonate groups are aligned in rows with all the carbonate groups pointing in the same direction in each row. Adjacent rows of carbonate groups lie with the carbonate group rotated by  $60^\circ$ . The structure of calcite II is derived from calcite I by rotating each carbonate group by a small amount (up to around  $11^\circ$  at the transition from calcite I) in the opposite direction to its adjacent groups. The results from simulations using all models show that the rotation continues to increase as pressure increases until a third stable phase is observed where the carbonate groups point in the same direction to their adjacent groups (Fig. 3).

To see the behaviour of the models through the phase changes, the models were allowed to relax at a range of pressures starting from calcite I, calcite II and the highest-pressure phase. The angle of the  $\text{CO}_3$  group relative to its orientation in calcite I is used as the order parameter to show the phase changes in Fig. 4. When started from different structures, the transitions often occur at different pressures. This is due to an optimized

**Table 1** Optimised potentials used for this work. Note that forces acting on the core rather than the shell of an atom are not conventional within GULP, the warnings should be ignored

Functional form	Bond	Coefficients			Cut off (Å)			
		A (eV)	$\rho$ (Å)	C (eV Å <sup>6</sup> )	Min	Max		
Buckingham (Eq. 2)	Ca–O shell	2404.3463	0.289118	0	0	10		
	Co–O shell	2300	0.254998	0	0	10		
	Zn–O shell	2300	0.256152	0	0	10		
	Cd–O shell	2300	0.278795	0	0	10		
	Ni–O shell	2300	0.250237	0	0	10		
	Mn–O shell	2300	0.267687	0	0	10		
	Sr–O shell	2300	0.304957	0	0	10		
	Mg–O shell	2300	0.257449	0	0	10		
	Fe–O shell	2300	0.262561	0	0	10		
	Ba–O shell	2300	0.322133	0	0	10		
	Pb–O shell	2300	0.309616	0	0	10		
	O shell–O shell	214836.21	0.198340	70.169	0	15		
	O–O	4030.3000	0.245497	0	Applies only within CO <sub>3</sub> group			
Morse (Eq. 3)	O–C	D (eV) 5	A (Å <sup>-1</sup> ) 2.5155	r <sub>0</sub> (Å) 1.20246	Applies only within CO <sub>3</sub> group			
Three-body (Eq. 4)	O–C–O	K <sub>2</sub> (eV/rad <sup>2</sup> ) 1.7887	$\theta_0$ 120°	Applies only within CO <sub>3</sub> group				
Torsional (Eq. 5)	O–C–O–O	K (eV) 0.15100	$\phi_0$ 0°	Applies only within CO <sub>3</sub> group				
Spring (Eq. 1)	O–O shell	K <sub>2</sub> (eV/Å <sup>2</sup> ) 20.673989	K <sub>4</sub> (eV/Å <sup>4</sup> ) 10000.000	Applies between oxygen and its shell				
Charges		Charge (e)		No cutoff				
Coulomb interaction	C core	+ 1.448759						
	O core	+ 0.2330047						
	O shell	-1.382591						
	Cation core	+ 2						

**Table 2** Comparison of generated and experimental physical parameters for calcite and aragonite

	Aragonite		Calcite	
	Experimental	Calculated	Experimental	Calculated
Elastic constants (Gpa)				
C <sub>11</sub>	85.0 <sup>a</sup>	130.8	145.7 <sup>b</sup>	151.9
C <sub>22</sub>	159.6 <sup>a</sup>	209.4		
C <sub>33</sub>	87.0 <sup>a</sup>	123.0	85.3 <sup>b</sup>	96.0
C <sub>44</sub>	42.7 <sup>a</sup>	41.7	33.4 <sup>b</sup>	45.3
C <sub>55</sub>	41.3 <sup>a</sup>	56.5		
C <sub>66</sub>	25.6 <sup>a</sup>	37.2		
C <sub>12</sub>	15.9 <sup>a</sup>	41.4	55.9 <sup>b</sup>	65.1
C <sub>13</sub>	36.6 <sup>a</sup>	58.3	53.5 <sup>b</sup>	62.7
C <sub>14</sub>			-20.5 <sup>b</sup>	22.1
C <sub>23</sub>	2.0 <sup>a</sup>	68.3		
Cell Parameters				
Volume (Å <sup>3</sup> )	226.9 <sup>f</sup>	228.70	367.8 <sup>e</sup>	365.26
a (Å)	5.740 <sup>f</sup>	5.73	4.990 <sup>e</sup>	4.97
b (Å)	4.961 <sup>f</sup>	5.00	4.990 <sup>e</sup>	4.97
c (Å)	7.967 <sup>f</sup>	7.98	17.061 <sup>e</sup>	17.08
Static dielectric				
11			8.5 <sup>c</sup>	6.50
22				
33			8 <sup>c</sup>	6.20
High-frequency dielectric				
11	2.86 <sup>d</sup>	1.84	2.75 <sup>d</sup>	1.75
22	2.82 <sup>d</sup>	1.65		
33	2.34 <sup>d</sup>	1.65	2.21 <sup>d</sup>	1.85

<sup>a</sup> Experimental values from Hearmon (1946)

<sup>b</sup> Experimental values from Dandekar and Ruoff (1968)

<sup>c</sup> Experimental values from Kaye and Laby (1982)

<sup>d</sup> Experimental values from Deer et al. (1966)

<sup>e</sup> Experimental values from Effenberger et al. (1981)

<sup>f</sup> Experimental values from De Villiers (1971)

structure being at a stationary point in the energy such that no net force acts on the atoms. For example, if the simulation was started from the calcite I structure and

the pressure increased, the phonon at the wave vector [½ 0 2] softens and above the transition point its frequency becomes imaginary. Although the calcite I

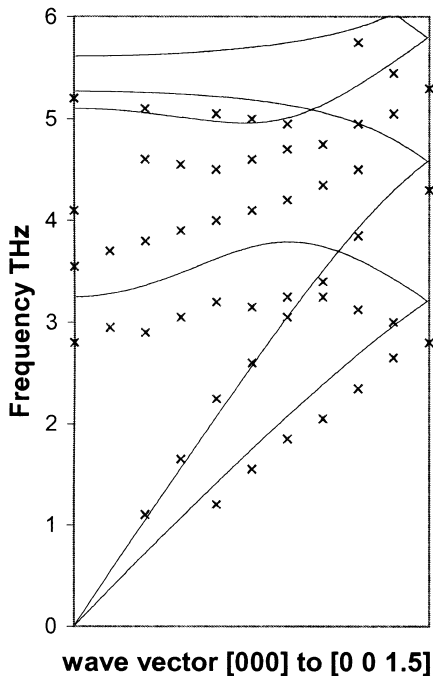


**Fig. 1** Comparison of experimentally determined (Cowley and Pant 1973 crosses) and calculated phonon dispersion curve between wave vectors [0 0 0] and [0 0 1.5] for the calcite I unit cell

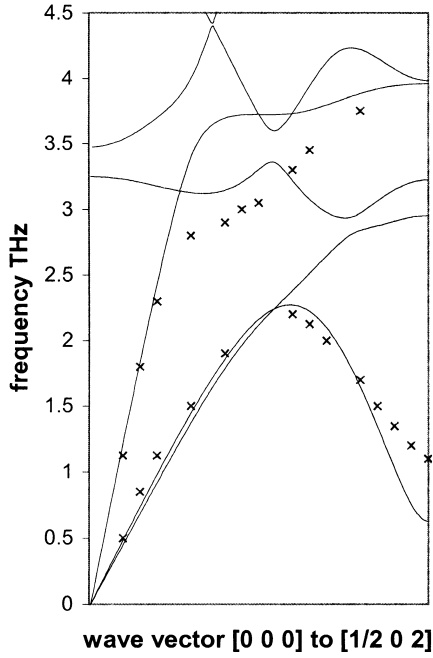


**Fig. 2** Phonon dispersion curve for K points between [0 0 0] and [1/2 0 2] in the calcite I unit cell. The crosses represent experimental results of Cowley and Pant (1973) whereas the lines were generated using the potentials from this study

structure is unstable, it remains at a potential maximum where no forces act on the atoms. All the transitions we observe in the computational models are due to rounding errors tipping the balance and causing the phase change. It is therefore meaningless to talk about the

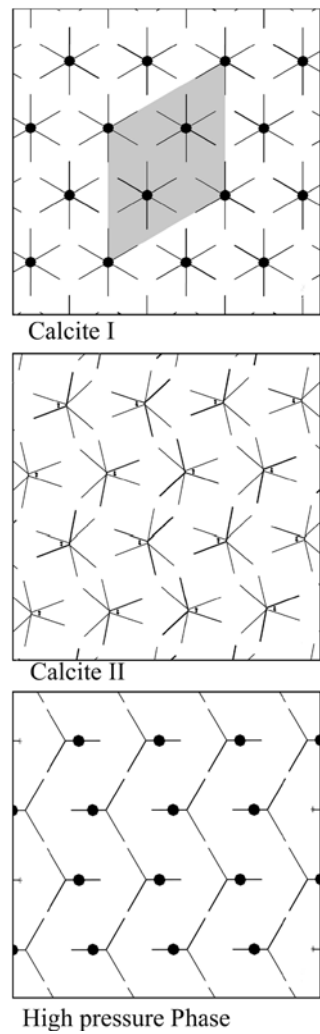
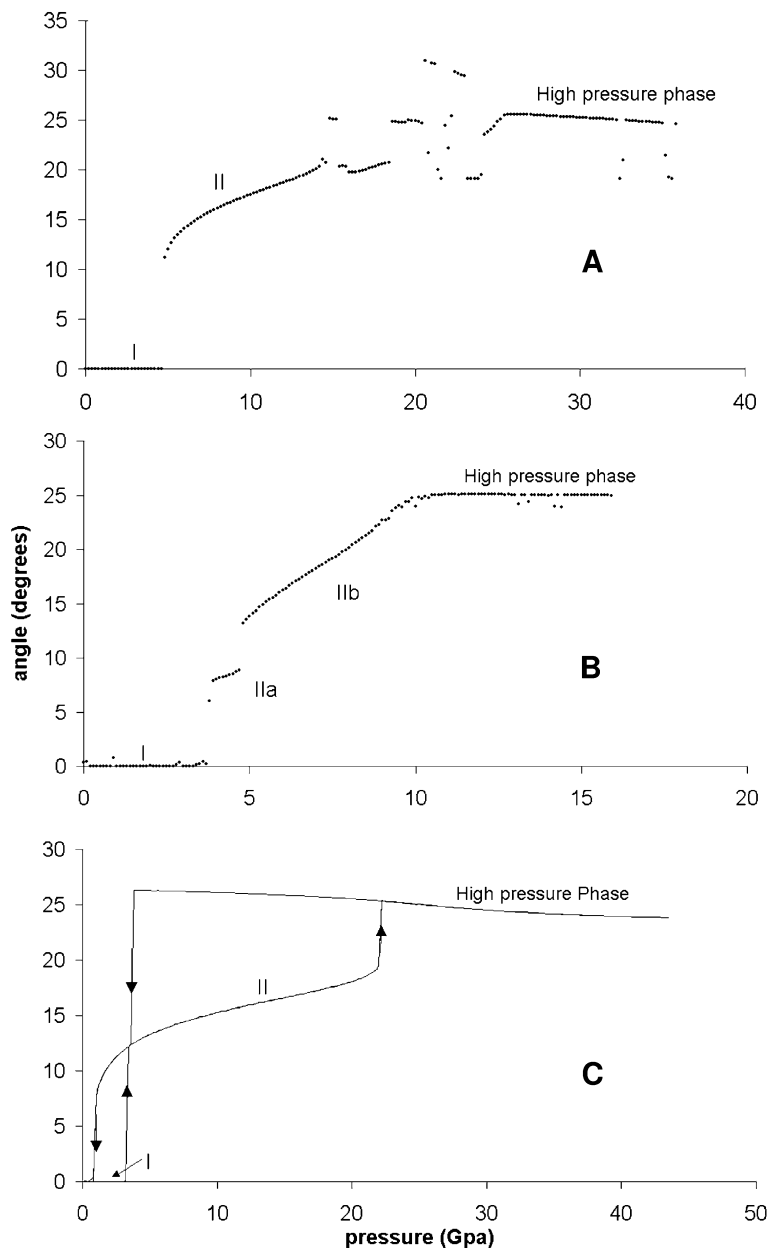


**Fig. 3** Calcium carbonate phases generated with the empirical potentials from this study, viewed perpendicular to the plane of the carbonate group

hysteresis of the transitions observed by starting the simulation from different structures. We will therefore discuss the transition point as where it becomes energetically favourable to be in a particular structure. However, by starting from different structures the nature of the transition can be mapped out.

The model produced by Dove et al. 1992b indicates that calcite undergoes a first-order phase transition from calcite I to calcite II at a pressure of 4.8 Gpa. This can be recreated by optimizing the calcite-II structure at a range of pressures. At higher pressures, a transition to the high-pressure phase is observed. Although the high-pressure phase was created using this model, the structure does not appear to optimize correctly between 15 and 25 Gpa, not allowing a characterization of the transition to the high-pressure phase of calcite. As the model does not have a shell it is very rigid in its behaviour. The program may not be able to find a potential minimum, due to the lack of cushioning that a shell offers.

**Fig. 4A–C** Rotation of the  $\text{CO}_3$  group relative to its position in calcite I for models Dove et al. (1992) (A), Pavese et al. 1996 (B) and the empirical model created in this study (C)



Using the potential produce by Pavese et al. (1996) four phases are observed: calcite I, calcite IIa, calcite IIb and a high-pressure phase. Calcite I is energetically favourable below 3.8 GPa, where a first-order transition to calcite IIa occurs. The transition to calcite IIb occurs at 4.7 GPa. The high-pressure phase becomes energetically favourable at pressures above 10.1 GPa, the transition from calcite IIb to the high-pressure phase is a second-order transition. The polymorphs calcite IIa and calcite IIb both have the structure of calcite II with differing degrees of  $\text{CO}_3$  group rotation. The reason for separating them is due to a discontinuity in the rotation of the carbonate group (Fig. 4). These transitions were observed by optimizing the calcite II structure at a range of pressures. Optimizing the structure of calcite I did not

generate other polymorphs, since there was insufficient numerical noise to lower the symmetry.

Using the potentials created in this study to model the structural transitions as a function of pressure, we find a first-order phase transition between calcite I and calcite II at 3.2 Gpa. A second, first-order transition occurs between calcite II and the highest pressure phase at 22.2 Gpa. Table 3 and 4 contain structures of calcite II and the high-pressure phase generated with these potentials. During the analysis of the structure and lattice energy of  $\text{CaCO}_3$  as a function of pressure we were unable to produce the suggested structure of calcite III given by Smyth and Ahrens (1997) with any of the models. The potentials did not show any other phonon softening in calcite I or II. This suggests that the

**Table 3** Comparison of calcite II experimental parameters from Merrill and Bussett (1975) with the structures generated at 1.8 and 3.2 GPa

	Experiment	1.8 GPa	3.2 GPa
Space group	P 1 21/c 1	P 1 21/c 1	P 1 21/c 1
<i>a</i>	6.334 Å	6.256465 Å	6.195155 Å
<i>b</i>	4.948 Å	4.995793 Å	4.98735 Å
<i>c</i>	8.033 Å	7.870953 Å	7.802957 Å
$\alpha$	90°	90°	90°
$\beta$	107.9°	107.325192°	106.965411°
$\gamma$	90°	90°	90°
Fractional coordinates			
Ca <i>x</i>	0.234	0.266694	0.231177
Ca <i>y</i>	0.738	0.759392	0.739528
Ca <i>z</i>	0.217	0.290759	0.202812
C <i>x</i>	0.26	0.23563	0.266337
C <i>y</i>	0.253	0.243327	0.242292
C <i>z</i>	0.504	0.507114	0.491412
O1 <i>x</i>	0.38	0.354657	0.402608
O1 <i>y</i>	0.156	0.076032	0.166562
O1 <i>z</i>	0.637	0.614247	0.635848
O2 <i>x</i>	0.134	0.100527	0.149476
O2 <i>y</i>	0.088	0.16004	0.068555
O2 <i>z</i>	0.381	0.365072	0.387677
O3 <i>x</i>	0.221	0.268667	0.227489
O3 <i>y</i>	0.49	0.489118	0.486186
O3 <i>z</i>	0.467	0.536677	0.457125

**Table 4** Structure of the high-pressure phase of calcite at 23 GPa, generated using the potentials from this study

Space group	P 1 21/m 1
<i>a</i>	5.514 Å
<i>b</i>	4.753 Å
<i>c</i>	3.9175 Å
$\alpha$	90°
$\beta$	105.81°
$\gamma$	90°
Fractional coordinates	
Ca <i>x</i>	0.2268
Ca <i>y</i>	0.75
Ca <i>z</i>	0.3608
C <i>x</i>	0.2709
C <i>y</i>	0.25
C <i>z</i>	0.9781
O1 <i>x</i>	0.196
O1 <i>y</i>	0.4754
O1 <i>z</i>	0.8272
O2 <i>x</i>	0.3854
O2 <i>y</i>	0.25
O2 <i>z</i>	1.2971

transition to calcite III is not a soft mode displacive phase transition.

### Defects in calcite and aragonite

The effects of cation defect substitutions were calculated using the Mott–Littleton method (1938). This method splits the lattice up into three regions determined by the distance from the defect centre. The first region incorporates the volume of the lattice closest to the defect. In this region, referred to as region 1, the lattice is allowed

to relax explicitly. In region 2a, the atoms are assumed to move harmonically around their equilibrium lattice position. In region 2b, the atoms respond only to the net Coulombic charge of the defect positioned at the defect centre. The size of each region is chosen by increasing its radius until the defect energy converges to within 2% of its extrapolated value at infinity. This was found to occur when region 1 has a radius of 10 Å.

In the model the only potential that acts on the cation is a Buckingham potential between the cation and the oxygen shell. Fixing the charge on the calcium ion at 2+ during fitting, allows other 2+ cations to be incorporated into the structure, provided we know the coefficients of the Buckingham interaction. The potentials of the defect cation were found by transferring the CO<sub>3</sub> group potentials to other carbonate phases and fitting against the experimental bulk modulus and structure. This procedure was implemented for a range of carbonates.

It was found that the *C* value of the Buckingham potential (Eq. 2) varied randomly, while the *A* value remained static when allowed to change during the fitting. An equal quality of fit was obtained by just fitting  $\rho$ . Fitting only the  $\rho$  parameter allowed a linear trend to be observed between the ionic radius of the cation and the value of  $\rho$ . This is expected, due to the form of the Buckingham potential.

$$v(r) = Ae^{-r/\rho} - Cr^{-6}. \quad (6)$$

The  $\rho$  value determines the width of the distribution, so the existence of this trend indicates that there are no other complications due to the change in orbital shape, which gives confidence that the model is working correctly. As the *A* and *C* value appear to be independent of the size of cation, the  $\rho$  value was refitted keeping the *A* and *C* values fixed to 2300 and 0 eV, respectively. Table 1 contains the parameters generated.

When one type of cation is replaced by another, the only effect on the model is to change the corresponding  $\rho$  value. The model does not distinguish between cations in any other manner. The observed trend between  $\rho$  and the ionic radius allows the model to predict the effect on the lattice of incorporation of an ion of any size (even ion sizes that do not exist). By running the simulation for a range of  $\rho$  values for effective cations in the calcite and aragonite structure, the defect energy trend lines in Fig. 5 were produced. Figure 5 also shows the calculated defect energies of real ions.

Smaller ions favour incorporation into the calcite structure over incorporation into the aragonite structure, but as the ion becomes bigger the difference in energy between defects in either structure decreases. For ions larger than 1.12 Å, there is a marginal preference for the aragonite structure.

To obtain an understanding of the energy difference it is first necessary to look at the effect each ion substitution has upon the lattice. Figure 6 shows defects of barium and nickel in the calcite I and aragonite structures.

**Fig. 5** Defect energy in calcite I and aragonite structures. The trend lines were generated by using the observed link between ion size and fitted  $\rho$  value; the trends were then created by substituting continuum of  $\rho$  values into the potential set

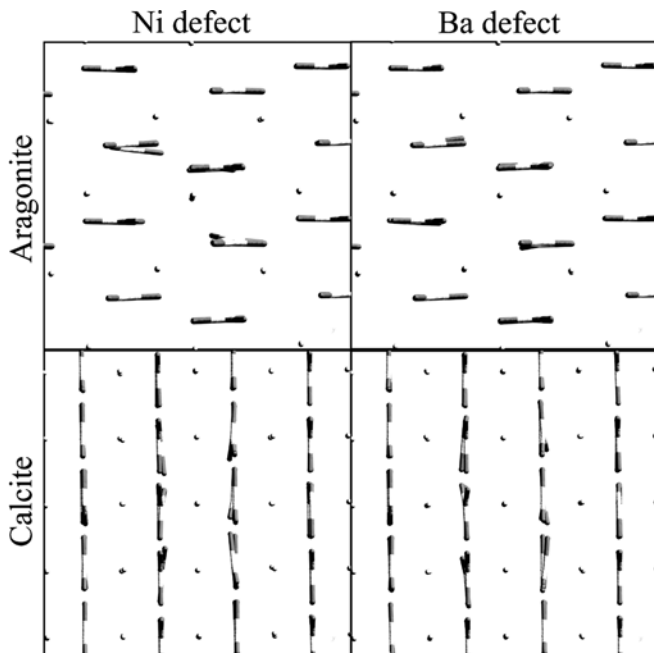
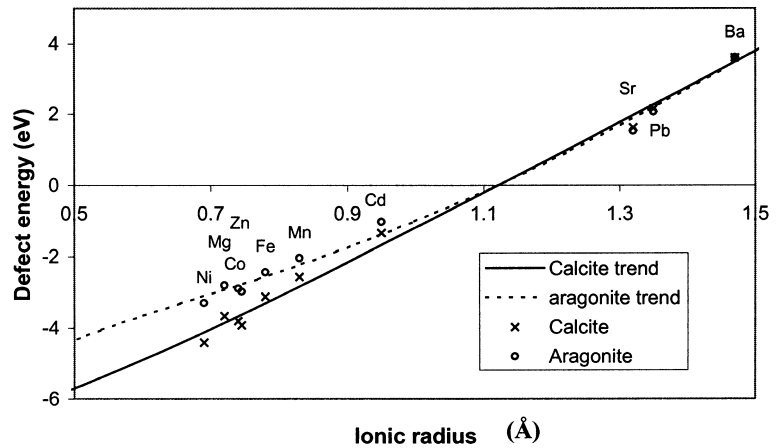


**Fig. 6** Distortion due to defects in calcite and aragonite structures, showing the observed asymmetrical distortion in aragonite comparison to the high symmetry of the distortions of the calcite structure

The barium ion is large and, as expected, distorts the structure of both aragonite and calcite more than a nickel ion. In the aragonite structure the difference is more pronounced. The Ni defect moves off its lattice position a lot more than the Ba ion. Due to the long range nature of the Coulomb potential, a distortion in the position of the cation dramatically increases the energy required to accommodate such a defect.

The details of the energy change arise from differences in the structure of calcite and aragonite. In calcite, the cations are equidistant to their nearest-neighbour oxygen atoms. Therefore, changing the size of the ion has no effect on its position, where the latter force must match the former. In aragonite the Buckingham force must match the Coulombic force. If the size of the ion is changed the ion must move, creating a dipole, which

distorts the crystal over a large volume, increasing the energy associated with the defect. The Buckingham potential with  $C = 0$  has the form:

$$U(r) = Ae^{-r/\rho} \quad (7)$$

The ratio of the force contribution of each cation's interaction with its first two nearest neighbours can therefore be written as:

$$\frac{F(r_1)}{F(r_2)} = \left[ e^{(\Delta r)} \right]^{\frac{-1}{\rho}}, \quad (8)$$

where  $r_1$  is the distance of the cation from the above plane of  $\text{CO}_3$  groups and  $r_2$  is the distance to the plane of  $\text{CO}_3$  groups below the cation and  $\Delta r$  is the difference between  $r_1$  and  $r_2$ .  $\rho$  becomes large as the ion size increases, causing the ratio of energy to approach 1. This mismatch in the Buckingham forces must be balanced by the Coulombic forces.

$$\left[ e^{(\Delta r)} \right]^{\frac{-1}{\rho}} = \frac{r_1^2}{r_2^2}. \quad (9)$$

Changing the  $\rho$  value must be balanced by moving the cation, thus creating a dipole. The Coulombic interaction has long-range effects, which create the difference between incorporating defects into calcite and aragonite. This approach oversimplifies the situation somewhat, but shows how the observed movement of the cation in aragonite can be identified as the cause of a significant portion of the difference between calcite and aragonite defect energies.

## Conclusions

Atomistic simulations in the Earth and material sciences allow observation of processes on the atomic scale, where direct laboratory measurements are difficult or impossible to perform. The improving technology in both code and computer speed allow the creation of larger, more accurate, models from which a better understanding of processes can be obtained. The main improvement of this work over previous models is to

incorporate the new interaction potentials between and within the carbonate molecular anions of Fisler et al. (2000) into a stable model.

By removing the instability in the model of Fisler et al. (2000), the potentials do not give as good an agreement with experimental data. This appears to be a step backwards; however, for the model to be used as a predictive tool it is necessary that it is stable. The refitted potential should therefore be used in all situations in preference to the model of Fisler et al. (2000). It is possible to refit the potentials and obtain better agreement with experimental parameters but for this potential structure such a refit results in degradation in the value of the soft mode.

The new empirical model for carbonates created in this work is stable for a wide range of carbonate structures and reproduces experimental results with a reasonable accuracy. Using the model at high pressure, calcite is observed to undergo two first-order phase transitions between calcite I, II and a high-pressure phase. No other instabilities or transitions are found. The defect energies of a range of substituting divalent cations in calcite and aragonite were calculated and the differences rationalized by observing differences in nearest-neighbour distances of the immediate coordination environment.

## References

- Bigg GR, Rohling EJ (2000) An oxygen isotope data set for marine waters. *J Geophys Res – Oceans* 105: 8527–8535
- Born M, Huang K (1954) Dynamical theory of crystal lattices. Oxford University Press, Oxford
- Catti M, Pavese A, Gale GD (1993) Therodynamic properties of  $\text{CaCO}_3$  calcite and aragonite: a quasi-harmonic calculation. *Phys Chem Miner* 19: 472–479
- Cowley ER, Pant AK (1973) Lattice dynamics of calcite. *Phys Rev (B)* 8: 4795–4800
- Dandekar DP, Ruoff AL (1968) Temperature dependence of the elastic constants of calcite between 160 and 300 K. *J Appl Phys* 39: 6004–6009
- Deer WA, Howie RA, Zussman J (1966) An introduction to rock-forming minerals. Longmans, London
- De Leeuw NH, Parker SC (2000) Modeling absorption and segregation of magnesium and cadmium ions to calcite surfaces: introducing  $\text{MgCO}_3$  and  $\text{CdCO}_3$  potential models. *J Chem Phys* 112: 4326–4333
- De Villiers JPR (1971) Crystal structures of aragonite, strontianite and witherite. *Am Mineral* 56: 758–767
- Dove MT, Powell BM (1989) Neutron-diffraction study of the tricritical orientational order-disorder phase transition in calcite at 1260. *Phys Chem Miner* 16: 503–507
- Dove MT, Hagen ME, Harris MJ, Powell BM (1992a) Anomalous inelastic neutron-scattering from calcite. *J Phys Condens Matter* 4: 2761–2774
- Dove MT, Winkler B, Leslie M, Harris MJ, Salje EKH (1992b) A new interatomic potential model for calcite – applications to lattice-dynamics studies, phase-transition and isotope fractionation. *Am Mineral* 77: 244–250
- Effenberger H, Mereiter K, Zeman J (1981) Crystal structure refinements on magnesite, calcite, rhodochrosite, siderite smithsonite and dolomite, with discussion of some aspects of the stereochemistry of calcite type carbonates. *Z Kristallogr* 156: 233–243
- Fisler DK, Gale JD, Cygan RT (2000) A shell model for simulation of rhombohedral carbonate minerals and their point defects. *Am Mineral* 85: 217–224
- Gale JD (1996) Empirical potential derivation for ionic materials. *Philos Mag B* 73: 3–19
- Gale JD (1997) GULP: a computer program for the symmetry-adapted simulation of solids. *J Chem Soc Faraday T* 93: 629–637
- Hearmon RFS (1946) The elastic constants of anisotropic minerals. *Rev Mod Phys* 18: 409–440
- Jensen F (2002) Introduction to computational Chemistry. John Wiley and Sons, New York, pp. 387–388
- Kaye GWC, Laby TH (1982) Tables of physical and chemical constants. Longman, London
- Merrill L, Bassett WA (1975) Crystal structures of  $\text{CaCO}_3$  (II) a high-pressure metastable phase of calcium carbonate. *Acta Crystallogr (B)* 31: 343–349
- Mott NF, Littleton MJ (1938) Conduction in polar crystals. I. Electrolytic conduction in solid salts. *J Chem Soc Faraday T* 34: 485–499
- Pavese A, Catti M, Price GD, Jackson RA (1992) Interatomic potentials for  $\text{CaCO}_3$  polymorphs (calcite and aragonite), fitted to elastic and vibrational data. *Phys Chem Miner* 19: 80–87
- Pavese A, Catti M, Parker SC, Wall A (1996) Modelling of the thermal dependence of structural and elastic properties of calcite,  $\text{CaCO}_3$ . *Phys Chem Miner* 23: 89–93
- Redfern SAT, Angel RJ (1999) High-pressure behaviour and equation of state of calcite,  $\text{CaCO}_3$ . *Contrib Mineral Petrol* 134: 102–106
- Singh AK, Kennedy GC (1974) Compression of calcite to 40 kbar. *J. Geophys Res* 79: 2615–2622
- Smyth JR, Ahrens TJ (1997) The crystal structure of calcite III. *Geophys Res Lett* 24: 1595–1598